JOURNAL OF GEOPHYSICAL RESEARCH, VOL. 98, NO. A7, PAGES 11,411–11,423, JULY 1, 1993

Theoretical Structure of a Magnetospheric Plasma Boundary: Application to the Formation of Discrete Auroral Arcs

M. ROTH

Institut d'Aéronomie Spatiale de Belgique, Brussels

D. S. EVANS

Space Environmental Laboratory, National Oceanic and Atmospheric Administration, Boulder, Colorado

J. LEMAIRE

Institut d'Aéronomie Spatiale de Belgique, Brussels

In the framework of a kinetic theory for tangential discontinuities we modeled the electrical structure of the sheath that separates magnetospheric particle populations of different densities and temperatures. The model can equally be applied to the plasma sheet boundary layer in the tail or to the boundary of some plasma sheet cloud immersed in the central plasma sheet. With plasma parameters typical of the Earth's outer magnetosphere and plasma sheet, we obtain results bearing many features pertinent to magnetospheric processes, specifically the origin of discrete auroral arcs. Creation of a space-charge separation electrostatic potential in a direction normal to the magnetic field results from the contact of the two plasma populations. When the large-scale solar wind potential difference is further imposed across the transition layer, the potential gradients are locally much enhanced, to give rise to large electric fields (several hundreds millivolts per meter) appearing over small distances perpendicular to the magnetic field—just the situation needed for the creation of an auroral arc. The transition itself is characterized by two scale lengths of the plasma and fields variables: the average electron Larmor radius ϱ_e (or some multiple of ϱ_e) for thin embedded electron-dominated layers which generate the sharpest potential gradients, and the ion gyroradius ρ_p (or some multiple of ρ_p) for the broader ion-dominated layers located at the outer edges of the transition. The larger-scale sizes are appropriate to auroral arcs dimensions. The generated electric potential differences, consistent with the energy acquired by the precipitated electrons associated with discrete aurora, are identified with the source of the electromotive force (EMF) required for the auroral current circuit. Wave particle interactions are likely to scatter the electrons into the atmospheric loss cone, establishing the current system threading both the EMF and the ionosphere by means of field-aligned currents. The half lifetime of the transition is at least of the order of 1000 s. This is also the time interval during which dissipative processes will not alter significantly the available potential gradients of the initially unloaded EMF.

1. INTRODUCTION

Lyons et al. [1979], *Lyons* [1981], and *Lyons and Evans* [1984] found evidence from coordinated auroral and magnetospheric particle observations that discrete auroral arcs are often located along magnetic field lines, which map to locations at high altitude that mark the separation between different magnetospheric plasma populations. It is generally believed that these arcs arise because of magnetic-field-aligned potential differences which energize and precipitate magnetospheric electrons while retarding positive ions, so as to create a limited region of very enhanced energy flow to the atmosphere in the form of accelerated electrons (see, for example, *Lyons* [1992] for a recent review). It is further thought that the magnetic-field-aligned potential difference occurs as a result of the existence of an electromotive force (EMF) located in the magnetosphere, remote from the atmosphere. This EMF is an essential part of a three-dimensional current system that threads both the ionosphere and the EMF by means of field-aligned currents. In this picture the magnetic-field-aligned potential difference arises as a natural consequence of the requirement that the total potentials associated with the magnetospheric EMF be distributed around the external circuit in a fashion that insures a divergence free current system.

These facts, as well as earlier kinetic models of tangential discontinuities in collisionless plasmas by *Sestero* [1964, 1966], *Lemaire and Burlaga* [1976], *Roth* [1976, 1978, 1979, 1984], *Lee and Kan* [1979], and *Roth et al.* [1990] motivated the present application of kinetic plasma theory to the boundary separating magnetospheric plasma populations of differing plasma densities and temperatures. Although we do not know definitely where the various particle features in the geomagnetic tail map to in the ionosphere [*Parks et al.*, 1992], the present model can equally be applied to the plasma sheet boundary layer (PSBL) in the tail that, following *Eastman et al.* [1984], maps to discrete auroral arcs, or to the boundary of some plasma sheet "cloud" immersed in the central plasma sheet (CPS), another location, which has also been suggested for the mapping of discrete arcs [e.g., *Elphinstone et al.*, 1991; *Zelenyi et al.*, 1990]. We therefore loosely refer to the high-altitude plasma transitions where discrete aurora map as being "magnetospheric plasma

Paper number 93JA00156.
0148-0227/93/93JA-00156$05.00

boundary layers" between plasma sheet "clouds" and their magnetotail "background." We believe that the magnetospheric dc generator, or EMF, which sustains the dissipative current in the auroral circuit, should be identified with the potential differences generated across these magnetospheric plasma boundary layers (in this context dc means that these potentials and associated currents do not oscillate and reverse sign but is not to mean that the situation is totally time stationary). The analog of this magnetospheric dc generator is the contact potential difference produced at the interface between two metallic conductors at different temperatures. There are also other devices and physical mechanisms capable of producing, both in the laboratory and in space, large potential differences and electric current systems, for example, the dynamo effect arising from the relative motion of conductors or plasma clouds in the presence of a magnetic field. In the case of dynamo action in the magnetosphere the electric field is generally called the convection electric field and extends over the whole volume of the moving plasma. For plasma motions at velocities of less than 100 km/s in the presence of magnetic fields of 40 nT or less, this convection electric field ($\mathbf{E} = -\mathbf{V} \wedge \mathbf{B}$) does not exceed 4 mV/m. However, because the scale size of the plasma motions can be very large, the total potential differences involved may also be large; in excess of 100,000 V in the case of the solar wind's motion with respect to the Earth. In contrast, the charge separation thermoelectric field strengths treated in this paper can have very much larger values (100–200 mV/m) although such fields are confined to much thinner layers at the edges of plasma irregularities.

In section 2 we briefly summarize the basic features of our kinetic model. The numerical results for several illustrative cases that utilize typical magnetospheric plasma populations and reasonable geometries are presented in section 3. A discussion of these solutions, especially their applicability to magnetospheric and auroral processes, is given in the last section together with a summary.

2. A Kinetic Model of a Magnetospheric dc Generator

Let us now consider two regions of plasma separated by a thin diamagnetic current layer. The kinetic model used to describe this layer is an extension of that proposed by *Sestero* [1964] to describe collisionless plasma sheaths in the laboratory. Although the plasma sheet is rarely in a stationary state, we assume that the structure of the transition layer does not change significantly over the characteristic period of time required for an Alfven wave to traverse it. We also consider that the radius of curvature of the boundary layer is much larger than its characteristic thickness, which is of the order of a few ion gyroradii. Under these circumstances the plasma layer can be considered as planar. Every physical quantity depends then on one space coordinate only, say x, normal to the (y-z) plane of the layer. Since, in general, the magnetic field direction does not vary by more than 10° or 20° from one side of a transition layer to the other side, we consider that the direction of $\mathbf{B}$ does not change nor reverse across the transition layer, although the scalar magnitude of $\mathbf{B}$ may vary. We assume therefore that the magnetic field direction is everywhere parallel to the z axis. In this case, $\mathbf{B}$ is the curl of a vector potential directed along the y axis ($\mathbf{a} = a_y \mathbf{e}_y$). The partial electric current densities ($\mathbf{j}_{p,e}$) of the protons (p) and electrons (e) are then necessarily parallel to the y axis ($\mathbf{j}_{p,e} = j_{p,e}\mathbf{e}_y$). The electric field (as spatial gradient of the potential ϕ) is in the x direction ($\mathbf{E} = E_x \mathbf{e}_x$). Indeed, we assume that there is no mass flow across the surface of discontinuity in a frame of reference fixed with respect to the boundary layer ($V_x = 0$). In any frame of reference satisfying this condition, the plasma flow ($\mathbf{V}$) is then entirely in the (y-z) plane and we further assume that, at both $x = -\infty$ and $x = +\infty$ the flows have identical magnitudes and directions ($\mathbf{V}(x = -\infty) = \mathbf{V}(x = +\infty) = \mathbf{V}_\infty$). Without loss of generality we can further particularize the frame of reference, and have chosen one where $\mathbf{V}_\infty = 0$; i.e., the transition layer is modeled in a frame where the plasma is at rest when $x \to \mp\infty$.

Note that, for the configuration described above, the current density is perpendicular to the electric field. Therefore we are actually modeling the electric field structure for an "unloaded" source of EMF. However, to at least zero order, a description of the electric field structure for the case of an unloaded EMF will also represent the loaded case quite well. Indeed, the available potentials and field intensities will change only slightly in going from a situation of no load to a loaded situation where there is a component of the total current that is flowing parallel to $\mathbf{E}$ (so that $\mathbf{E} \cdot \mathbf{J} \neq 0$).

The Vlasov kinetic theory of the one-dimensional transition layer used in this paper (which is in effect a tangential discontinuity) is described in Appendix A. When $x \to \mp\infty$ it is assumed that the plasma, composed of protons and electrons, is described by Maxwellian velocity distribution functions. At any point inside the transition layer the velocity distribution functions correspond to the interpenetration of these two hydrogen plasmas in the form given by (A6). The plasma boundary conditions describe, on one side ($x \to -\infty$), a plasma sheet cloud (subscript c) with uniform number densities ($N_{ce} = N_{cp}$) and temperatures (T_{ce}, T_{cp}), and on the other side ($x \to +\infty$), a background magnetotail plasma (subscript b) with uniform number densities ($N_{be} = N_{bp}$) and temperatures (T_{be}, T_{bp}). In a collisionless plasma, the boundary conditions do not uniquely determine the transition profiles [*Sestero*, 1964]. The solutions (A6) describe just one Vlasov equilibrium among the many possible ones satisfying the same boundary conditions. Because the distribution of the particles in the six-dimensional space phase can be prescribed at will on certain characteristics of the Vlasov equation—those which do not intersect the hyperplanes at $x = \pm\infty$—the choice of the solutions should be made principally on the basis of mathematical simplicity. In particular, we would like all moments of the velocity distribution functions be analytical functions of ϕ and a_y. In Appendix B it is shown that this requirement is satisfied since the moments of (A6), in particular the partial number densities $n_e = n_{ce} + n_{be}$; $n_p = n_{cp} + n_{bp}$ and the partial current densities $j_e = j_{ce} + j_{be}$; $j_p = j_{cp} + j_{bp}$, are analytical functions of ϕ and a_y. The partial number densities are given by

$$n_{ce} = \frac{\alpha_{ce}}{2} \exp\left(+\frac{e\phi}{kT_{ce}}\right) \operatorname{erfc}\left(+\frac{a_y}{D_{ce}B_c}\right) \tag{1}$$

$$n_{cp} = \frac{\alpha_{cp}}{2} \exp\left(-\frac{e\phi}{kT_{cp}}\right) \operatorname{erfc}\left(+\frac{a_y}{D_{cp}B_c}\right) \tag{2}$$

$$n_{be} = \frac{\alpha_{be}}{2} \exp\left(+\frac{e\phi}{kT_{be}}\right) \operatorname{erfc}\left(-\frac{a_y}{D_{be}B_b}\right) \quad (3)$$

$$n_{bp} = \frac{\alpha_{bp}}{2} \exp\left(-\frac{e\phi}{kT_{bp}}\right) \operatorname{erfc}\left(-\frac{a_y}{D_{bp}B_b}\right) \quad (4)$$

and the partial current densities by

$$j_{ce} = -\alpha_{ce} e \sqrt{\frac{kT_{ce}}{2\pi m_e}} \left(\frac{\rho_{ce}}{D_{ce}}\right) \cdot \exp\left(+\frac{e\phi}{kT_{ce}}\right) \exp\left(-\frac{a_y^2}{D_{ce}^2 B_c^2}\right) \quad (5)$$

$$j_{cp} = -\alpha_{cp} e \sqrt{\frac{kT_{cp}}{2\pi m_p}} \left(\frac{\rho_{cp}}{D_{cp}}\right) \cdot \exp\left(-\frac{e\phi}{kT_{cp}}\right) \exp\left(-\frac{a_y^2}{D_{cp}^2 B_c^2}\right) \quad (6)$$

$$j_{be} = +\alpha_{be} e \sqrt{\frac{kT_{be}}{2\pi m_e}} \left(\frac{\rho_{be}}{D_{be}}\right) \cdot \exp\left(+\frac{e\phi}{kT_{be}}\right) \exp\left(-\frac{a_y^2}{D_{be}^2 B_b^2}\right) \quad (7)$$

$$j_{bp} = +\alpha_{bp} e \sqrt{\frac{kT_{bp}}{2\pi m_p}} \left(\frac{\rho_{bp}}{D_{bp}}\right) \cdot \exp\left(-\frac{e\phi}{kT_{bp}}\right) \exp\left(-\frac{a_y^2}{D_{bp}^2 B_b^2}\right) \quad (8)$$

In (1) through (8) erfc is the complementary error function, e is the magnitude of the electron charge, k is the Boltzmann constant, B_c and B_b are respectively the magnitude of the magnetic field deep in the plasma sheet cloud (at $x = -\infty$) and far from the transition in the magnetotail background (at $x = +\infty$). The parameters D_{ce}, D_{cp}, D_{be}, and D_{bp} characterize the "thickness" for each of the four transitions that the different particle populations undergo (see Appendix A). The sharpest transitions are obtained when

$$D_{ce} = \rho_{ce},\ D_{cp} = \rho_{cp},\ D_{be} = \rho_{be},\ D_{bp} = \rho_{bp} \quad (9)$$

where ρ_{ci} and $\rho_{bi} (i = e, p)$ are the asymptotic Larmor gyroradii defined in (A8). Taking account of the quasi-neutrality of the plasma and also that $a_y(x = -\infty) = -\infty$, $a_y(x = +\infty) = +\infty (B_z > 0)$, the parameters α_{ce}, α_{cp}, α_{be}, and α_{bp} are seen to be linked to the boundary conditions as follows:

$$\alpha_{ce} = \alpha_{cp} = n_e(x = -\infty) = n_p(x = -\infty) = N_{ce} = N_{cp} \quad (10)$$

$$\alpha_{be} \exp\left[+\frac{e\phi(x=+\infty)}{kT_{be}}\right] = \alpha_{bp} \exp\left[-\frac{e\phi(x=+\infty)}{kT_{bp}}\right] = n_e(x = +\infty) = n_p(x = +\infty) = N_{be} = N_{bp} \quad (11)$$

To find (10), it has been assumed that $\phi(x = -\infty) = 0$. The quantity $\phi_2 = \phi(x = +\infty)$ is then the electric potential difference across the transition. From (11) it can be seen that α_{be}, α_{bp}, or ϕ_2 can be chosen as arbitrary parameter, when the asymptotic densities at $x = +\infty$ (N_{be} and N_{bp}) are fixed.

The nonuniqueness of the velocity distribution functions, resulting from the collisionless and adiabatic nature of the interaction between the plasma particles is not entirely removed by the choice of the distributions (A6), since the model depends on five free parameters: D_{ce}, D_{cp}, D_{be}, D_{bp} and one among the three following ones: α_{be}, α_{bp} and ϕ_2 which are related to each other by (11).

The first four parameters define the sharpness of the transition. Their exact values can be chosen on the basis of both theoretical and observational facts. It is clear that the transition thickness is expected to scale according to some small microscopic parameter. In magnetized collisionless plasmas this small parameter is the particle Larmor radius, at least when the plasma is quasi-neutral. There are observational facts supporting this theoretical argument. For instance, high time resolution data of the plasma sheet boundary [*Parks et al.*, 1992] have shown that plasma parameters often vary on a scale length of the order of the ion Larmor radius, with encrusted electron structures of smaller thickness. Accordingly, the sharpest transitions defined by (9), which also correspond to the upper limits of plasma gradients, are not too far from those observed in the vicinity of the plasma sheet–lobe boundary.

To emphasize the effect of an external electric field transverse to the magnetic field (in the direction of the plasma gradients as in the theory of *Lyons* [1981]), the parameter ϕ_2 has been chosen as our fifth free parameter.

To find the structure of the transition layer as a function of x, we must solve Maxwell equations (in SI units):

$$\frac{d^2\phi}{dx^2} = -\frac{e}{\varepsilon_0}(n_{cp} + n_{bp} - n_{ce} - n_{be}) \quad (12)$$

$$\frac{d^2 a_y}{dx^2} = -\mu_0(j_{cp} + j_{bp} + j_{ce} + j_{be}) \quad (13)$$

where ε_0 and μ_0 are the vacuum permittivity and permeability, respectively.

The electric field E_x and the magnetic field B_z are the derivative of the potentials; i.e.,

$$E_x = -\frac{d\phi}{dx},\ B_z = +\frac{da_y}{dx} \quad (14)$$

The electric potential $\phi(x)$ must satisfy Poisson's equation (12). However, for nonrelativistic plasmas, where the characteristic thickness (D) is (much) larger than the Debye length (λ_D), *Roth et al.* [1990] have shown that a satisfactory first approximation for $\phi(x)$ is obtained by solving, iteratively, the charge-neutral approximation of Poisson's equation; i.e.,

$$n_{ce}(x) + n_{be}(x) = n_{cp}(x) + n_{bp}(x) \quad (15)$$

Roth et al. [1990] have shown that this approximation holds even for thin transitions with characteristic thickness of the order of the electron gyroradii—a scale which corresponds to the thinnest structure found in the transition layers studied in this paper. The Laplacian of $\phi(x)$ (i.e., $d^2\phi/dx^2$)

TABLE 1. Boundary Conditions on Both Sides of a Magnetospheric Plasma Transition Layer

N_{ce}	T_{ce}	N_{cp}	T_{cp}	N_{be}	T_{be}	N_{bp}	T_{bp}	B_c
0.5 cm^{-3}	2500 eV	0.5 cm^{-3}	12000 eV	0.15 cm^{-3}	800 eV	0.15 cm^{-3}	3000 eV	40 nT

Subscripts c and b are for conditions, respectively, deep in the plasma sheet cloud (at $x = -\infty$) and far from the transition in the magnetotail background (at $x = +\infty$). Subscripts e and p are respectively for electrons and protons.

can be calculated to estimate the value of the actual charge separation relative density

$$\frac{dQ}{|Q|}(x) = -\frac{\varepsilon_0}{en_p(x)}\frac{d^2\phi}{dx^2}(x) \tag{16}$$

It will be shown (a posteriori) in section 3 that the $dQ/|Q|$ is indeed a small quantity throughout the whole plasma sheath; i.e., that (15) is a valid zero-order approximation and substitute for Poisson's equation.

The magnetic and electric field distributions are finally determined by solving (13)–(15), with the partial number densities and currents given by (1)–(8). Equation (13) is solved by using a Hamming's predictor-corrector scheme. It is coupled with (15), whose solution is obtained by Newton-Raphson method for finding the root of a nonlinear algebraic equation. In practice, one starts integrating with a large negative value of a_y so that the asymptotic moments of the velocity distribution functions at $x = -\infty$ are reached.

In section 3 we first present the numerical solution to (13)–(15) for an illustrative case that uses typical magnetospheric plasma densities and temperatures and the imposed boundary condition that the total potential across the system (ϕ_2) equals zero. In section 3 we also discuss a wider family of solutions for cases where this boundary condition is relaxed and large-scale electric potentials applied across the system—arising for example from the solar wind induced dawn-dusk electric field—are permitted. The second class of solutions has the interesting property that the large scale applied electric field, which is uniform in the absence of plasma structures internal to the system, becomes highly concentrated at the boundary between plasmas when such boundaries exist. Both sets of solutions correspond to the sharpest structures defined by (9).

3. Numerical Results

Table 1 gives the plasma characteristics far from ($x \to \mp\infty$) the transition layer assumed for this study. Also given in Table 1 is B_c: the assumed magnetic field strength deep in the plasma sheet cloud ($x \to -\infty$). The plasma temperatures, plasma densities, and magnetic field strength are

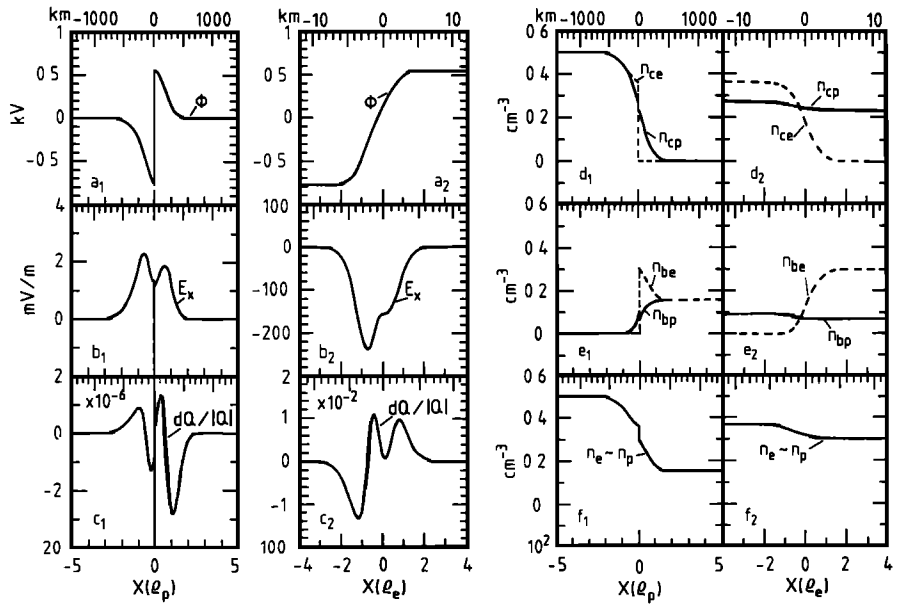

Fig. 1. Structure of a transition layer for which the potential difference $\phi_2 = 0$. Boundary conditions typical in the Earth's outer magnetosphere and plasma sheet are given in Table 1. At the outer edges of this potential layer (see panels of the first and third columns displayed on the ϱ_p scale), the average proton gyroradius ($\varrho_p = (\rho_{cp} + \rho_{bp})/2 \approx 280$ km) is the representative scale length, while the middle of the transition (see panels of the second and fourth columns displayed on the ϱ_e scale) is dominated by a very thin structure, whose scale length is the average electron gyroradius [$\varrho_e = (\rho_{ce} + \rho_{be})/2 \approx 3$ km]. In the two left-hand side panels the following variables are successively displayed (from top to bottom): the electric potential ϕ; the electric field E_x and the charge separation relative density $dQ/|Q|$. In the two right-hand side panels we display, from top to bottom: the electron n_{ce} and proton n_{cp} number densities of the plasma sheet cloud particles; the electron n_{be} and proton n_{bp} number densities of the magnetotail background and the total electron n_e and proton n_p number densities. The distance x across the planar surface of interface is also shown in kilometer by the upper scales.

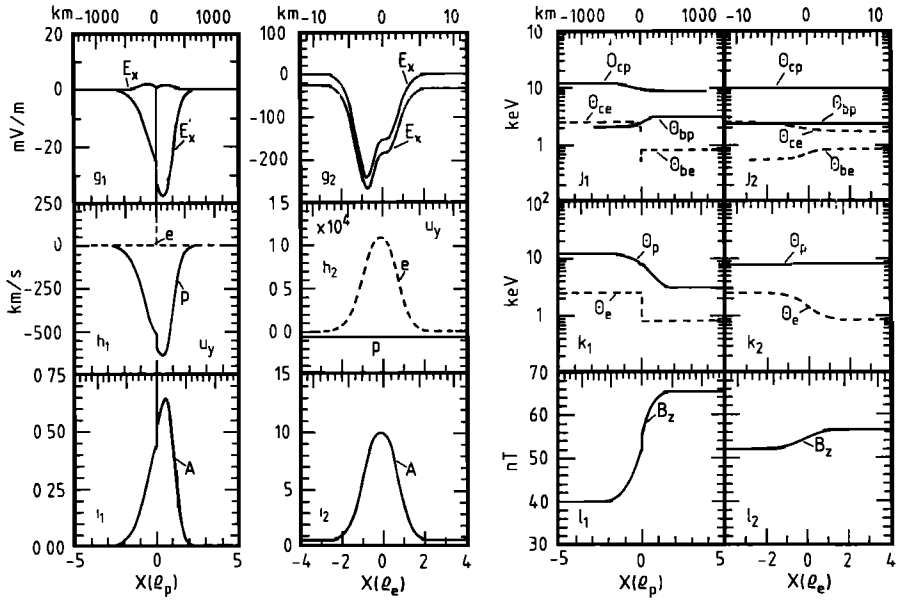

Fig. 2. Structure of a transition layer for which the potential difference $\phi_2 = 0$. Boundary conditions typical in the Earth's outer magnetosphere and plasma sheet are given in Table 1. At the outer edges of this potential layer (see panels of the first and third columns displayed on the ϱ_p scale), the average proton gyroradius ($\varrho_p = (\rho_{cp} + \rho_{bp})/2 \approx 280$ km) is the representative scale length, while the middle of the transition (see panels of the 2nd and 4th columns displayed on the ϱ_e scale) is dominated by a very thin structure, whose scale length is the average electron gyroradius ($\varrho_e = (\rho_{ce} + \rho_{be})/2 \approx 3$ km). In the two left-hand side panels the following variables are successively displayed (from top to bottom): the electric field both in the stationary (x-y-z) frame (E_x) and in the plasma frame ($E'_x = E_x + V_y B_z$); the electron (e) and proton (p) average velocity u_y and the ratio $A = |u_{y,p} - u_{y,e}|/U_p$, where U_p is the average thermal ion speed: $U_p = (k\theta_p/m_p)^{1/2}$ ($A = 1$ corresponds to the threshold for the modified two-stream instability). In the two right-hand side panels we display, from top to bottom: the individual temperature of the electrons θ_{ce} and protons θ_{cp} of the plasma sheet cloud and of the electrons θ_{be} and protons θ_{bp} of the magnetotail background; the average temperature of the electrons θ_e and protons θ_p and finally the magnetic field B_z. The computation of the partial temperatures (θ_{ce}, θ_{cp}, θ_{be}, θ_{bp}) was stopped when the corresponding number densities became so small that even the notion of temperature was meaningless. The distance x across the planar surface of interface is also shown in kilometer by the upper scales. The thin electron layer is unstable with respect to the modified two-stream instability. Indeed the instability threshold A exceeds unity in this narrow region where extremely large (and unstable) E fields are generated.

typical of conditions likely to be found in the Earth's outer magnetosphere and plasma sheet. Actually, we derived the electron number densities and temperatures from rocket data showing a discontinuity in the inferred temperatures and densities of the parent magnetospheric plasma at the edge of an auroral arc [*Lyons et al.*, 1979; *Lyons*, 1981]. The ion temperatures were estimated on the premise that ion temperatures in the plasma sheet are typically 4–5 times higher than the electron temperatures. We modeled the electrical and plasma structure of the transition layer using data from Table 1 both for the case when the large-scale, externally applied potential across the system is zero and for cases when this applied potential is non-zero (for example, because of the solar wind's interaction with the geomagnetic field).

Figures 1 and 2 illustrate the numerical solution for the electrical and plasma structure across the transition between the two assumed plasma populations for the case where ϕ_2, the externally applied potential across the system, is 0 V. It can be seen that two different scale lengths characterize the structure of the transition. At the outer edges of the transition layer the average ion gyroradius [$\varrho_p = (\rho_{cp} + \rho_{bp})/2 \approx$ 280 km] is the representative scale length, while the average electron gyroradius [$\varrho_e = (\rho_{ce} + \rho_{be})/2 \approx 3$ km] dominates the middle of the transition. This very thin structure—about 4 electron gyroradii thick—is mainly an electron-dominated layer, i.e., a layer dominated by the electron current. This layer is illustrated in panels of the second and fourth columns. Panels of the first and third columns illustrate the characteristics of two much thicker transitions, dominated by the ion current. These ion-dominated layers are separated by the thin electron-dominated layer located near $x \approx 0$.

In Figure 1 it can be seen that the potential difference across the electron-dominated layer is about 1350 V (see panels a_1 and a_2). In the two ion-dominated layers, located at the outer edges of the transition layer, the plasma density gradient is parallel to the potential gradient (see panels a_1 and f_1). This is not the case in the electron layer, near $x \approx 0$, where the gradient of the electric potential is opposite to the density gradient (see panels a_2 and f_2) and has a different direction than on both sides in the proton layer. This is illustrated in the next panels (b_1 and b_2) showing the electric field intensity E_x which is perpendicular to the surface of the plasma layer. E_x has a peak value of -220 mV/m inside the electron-dominated layer (see panel b_2) but does not exceed 2.5 mV/m inside the ion-dominated layers (see panel b_1). The relative electric space charge density deduced from (16) is given in panels c_1 and c_2. It can be seen that $|dQ/Q|$ is smaller than 2% within the electron-dominated layer and smaller than 3×10^{-6} in the adjacent ion-dominated layers. This confirms a posteriori that charge neutrality is satisfied to a very good approximation. This

confirms also that the solution of (15) is a satisfactory approximation for the electric potential distribution throughout the whole transition. When (15) is replaced by

$$n_{cp}(a_y^{(1)}, \phi^{(1)}) + n_{bp}(a_y^{(1)}, \phi^{(1)}) - n_{ce}(a_y^{(1)}, \phi^{(1)}) - n_{be}(a_y^{(1)}, \phi^{(1)}) = -\frac{\varepsilon_0}{e}\frac{d^2\phi^{(0)}}{dx^2}(a_y^{(1)}, \phi^{(1)}, B_z^{(1)}) \quad (17)$$

where $\phi^{(0)}$ is the solution of (15), *Roth et al.* [1990] have shown that the first-order solution for the electric potential $\phi^{(1)}$ is not significantly different that the one shown in Figure 1, even in the very thin electron-dominated layer where the first-order solution differed from the quasi-neutral solution by less than 1 part in 100. Moreover, the small change in the modeled electrostatic structure of the layer between the quasi-neutral and first-order solutions made virtually no difference to modeled magnetic field distribution.

The partial number densities of particles from the plasma sheet cloud (n_{ce} and n_{cp}) are illustrated in panels d_1 and d_2, while those of particles from the background magnetotail are illustrated in panels e_1 and e_2. The total number density of electrons (n_e) and protons (n_p) is displayed in panels f_1 and f_2. From these figures it can be seen that the two different electron populations (c and b) interpenetrate mainly in the thin electron layer, near $x \approx 0$; while the two proton populations interpenetrate in a sheath of 2 ϱ_p thick centered near $x \approx 0$.

In panels g_1 and g_2 of Figure 2, it is interesting to note that E'_x, the electric field in the frame of reference comoving with the plasma ($E'_x = E_x + V_y B_z$), takes large values, even in the ion-dominated layers ($E'_x \approx -30$ mV/m). This means that the ideal MHD approximation is not applicable here. In the electron-dominated layer, (see panel g_2), $E'_x \approx E_x$ and the electric field E_x is mainly a charge separation electric field.

The average velocity of the protons $u_{y,p}$ and electrons $u_{y,e}$ is displayed in panels h_1 and h_2 of Figure 2 [$u_{y,i} = (n_{ci}u_{y,ci} + n_{bi}u_{y,bi})/(n_{ci} + n_{bi})$ where $i = e, p$]. In panel h_1, note the large ion jets velocity of more than 500 km/s. These jets are parallel to the plasma sheath and perpendicular to the magnetic field, and occur on a scale length of about 300 km in the direction normal to the transition layer. As might be expected, these ion jets represent the main contribution to the electric current in the ion-dominated layers. In these layers, there is a weak charge separation electric field (≈2 mV/m—see panel b_1 of Figure 1). This field is due to the charge distribution shown in panel c_1 (Figure 1), where it can be seen that a pair of charge layers develop across each ion-dominated transition region where the two plasmas of different origins interpenetrate. At the edges of these ion-dominated layers, the protons are deflected transversely by the magnetic field. They acquire thus a large transverse velocity $u_{y,p}$ parallel to the sheath ($u_{y,p} \approx -500$ km/s), that is nearly equal to their thermal speed. At these locations, their average velocity greatly exceeds that of the electrons (see panel h_1).

Even more surprising is the narrow jet sheath of electrons with a velocity of the order of 10,000 km/s near $x \approx 0$ (see panel h_2). This jet represents the main contribution to the electric current in the electron-dominated layer near $x \approx 0$. In this layer, a strong polarization electric field (≈ −200 mV/m—see panel b_2 of Figure 1) perpendicular to the magnetic field is present. It is generated by very thin charged layers: a layer of negative charges near $x \approx -\varrho_e$ and two layers of positive charges near $x \approx -0.5\varrho_e$ and $x \approx \varrho_e$ (see panel c_2 of Figure 2 showing $dQ/|Q|$). The strong electric field near $x \approx 0$ arises from the slight charge imbalances in the electron-dominated layer and serves to prevent still greater charge imbalance thus preserving the quasi-neutrality condition. The electrons are accelerated by this strong electric field in a direction normal to the sheath and are finally turned around by the magnetic field just as they attain a maximum kinetic energy, a fraction of the thermal energy of the ions. Therefore these electrons acquire a very large velocity ($u_{y,e}$) parallel to the sheath (≈10,000 km/s) that greatly exceeds that of the ions.

Instabilities can be expected to relax the strong gradients in both the plasma density and flows illustrated in panels f_1 (Figure 1) and h_1 (Figure 2). Potential candidates are current-driven lower hybrid instabilities like the modified two-stream instability [*McBride et al.*, 1972; *Wu et al.*, 1983] or the lower hybrid drift instability [*Davidson et al.*, 1977; *Huba et al.*, 1978]. In the ion-dominated layers located at the outer edges of the transition layer, the lower hybrid drift instability which is driven by the ion diamagnetic current, could contribute to a wave spectrum near the lower hybrid frequency. Modes driven by the electron cross-field current are also expected to be unstable in the thin electron-dominated layer near $x \approx 0.$, where the electron cross-field current largely exceeds the proton diamagnetic current. In this electron layer the modified two-stream instability, which is driven by relative streaming of electrons and ions across **B**, can be expected to contribute most to the electrostatic noise near the lower hybrid frequency; although the electron-ion hybrid mode recently analyzed by *Romero et al.* [1992] can also contribute to the wave spectrum (this mode, being driven by velocity shear and independent of the plasma current, cannot be identified with the two-stream instability). The ratio

$$A(x) = \frac{|u_{y,p}(x) - u_{y,e}(x)|}{U_p(x)}, \quad U_p(x) = \sqrt{\frac{k\theta_p(x)}{m_p}} \quad (18)$$

where $U_p(x)$ is the average thermal speed of protons with average temperature $\theta(x)$—is linked to the modified two-stream instability threshold. Following *McBride et al.* [1972], the threshold is attained when $A \geq A_0 \approx 1$. With this criterion, the thin electron-dominated layer near $x \approx 0$ is indeed expected to be highly unstable since $A \gg 1$ (see panel i_2 of Figure 2) and is likely to produce large-amplitude electrostatic wave noise. These waves can then interact with the electrons by changing their pitch angle distribution. Note that the maximum growth rate of the most unstable modes is high, probably of the order of the lower hybrid frequency [*McBride et al.*, 1972]. This means that, as long as the density and temperature gradients are maintained, the wave activity is turned on and is a very fast and efficient scattering mechanism. It could however be that, as a result of this wave-particle interaction, the initial electron velocity distribution becomes less anisotropic, hence leading to a broadening of the electron-dominated layer. The final configuration can eventually be one where the initial "thickness" $D_{ce} = \rho_{ce}$ and $D_{be} = \rho_{be}$ are enlarged to become of the order of

multiples of ρ_{ce} and ρ_{be}. Such enlarged electron layers (scale size 50 km) and broadband electrostatic noise are common features observed in the PSBL [*Parks et al.*, 1992]. The observation of this electrostatic noise indicates that these enlarged electron layers still generate enough wave power to scatter electrons into the loss cone at a rate sufficient to maintain an auroral activity.

The partial temperatures (θ_{ce}, θ_{cp}, θ_{be}, θ_{bp}) are shown in panels j_1 and j_2 of Figure 2. The computation of these temperatures was stopped when the partial number densities became so small that even the concept of temperature was meaningless. These quantities have been computed from (B20), (B24), and (B25). From these equations, only the temperature along the y axis contributes to the variation of θ across the layer. The panels k_1 and k_2 (Figure 2) illustrate the average electron (θ_e) and proton (θ_p) temperatures: $\theta_i = (n_{ci}\theta_{ci} + n_{bi}\theta_{bi})/(n_{ci} + n_{bi})$, $i = e, p$. It can be seen that these temperature distributions reflect a boundary transition from a hot plasma sheet cloud to a cooler magnetotail background in keeping with the boundary conditions given in Table 1.

The panels l_1 and l_2 (Figure 2) illustrate the diamagnetic effect due to the surface currents around the plasma sheet cloud. Inside the cloud, the decrease of the magnetic pressure is balanced by an equivalent increase in the kinetic plasma pressure, since the sum of the magnetic and kinetic pressures does not vary across the sheath.

The results shown in Figure 1 and 2 are appropriate for the case where there is no large-scale potential difference externally imposed across the system. However, the boundary condition at $x = +\infty$ given by (11) permits the relaxation of this condition. In the theory of *Lyons* [1981], this external potential difference (ϕ_2) is the source of the auroral EMF. Such an additional potential drop will biase the electric potential distribution. It can either sharpen or attenuate the electric potential gradient inside the transition layer as shown in Figure 3. This figure displays the solution for the electrical structure of a transition region between plasmas when potentials of +3500, −1650, and −3500 V have been externally applied from $+\infty$ to $-\infty$ across the system. The results for zero applied potential, discussed earlier, are also plotted in Figure 3 for comparison. The plasma and magnetic field properties assumed for this calculation are the same as given in Table 1. The left-side panels in Figure 3 characterize the ion-dominated layers, located at the extreme edges of the transition, while the right-hand panels pertain to the electron-dominated layer near $x \approx 0$.

The most striking feature of the potential distributions across these plasma boundaries is that the great bulk of the available electric potential difference appears over a small-scale size at the location of the boundary. In effect, the presence of plasma boundaries in the system concentrates imposed electric fields and gives rise to localized potential differences much larger than that produced by the contact between the two plasmas alone (see Figure 1). The actual potential differences available in the magnetosphere because of the solar wind's interaction with the geomagnetic field often exceed 100,000 V, but the exact value will depend on the amount of intervening structure between the magnetotail boundary layer and the solar wind. Furthermore, the plasmas in the outer magnetosphere are known to be highly structured with both gross scale structures (e.g., the boundary layer of the plasma sheet) and small-scale internal

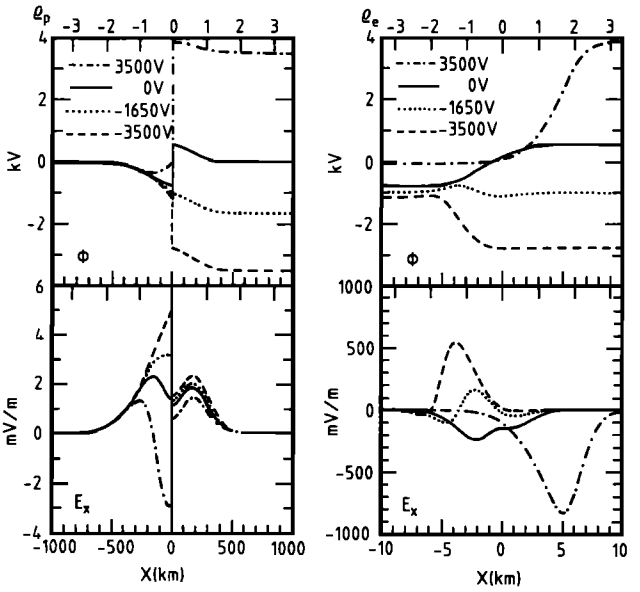

Fig. 3. Electric potential ϕ and electric field E_x structures for different values of the potential difference (ϕ_2 = 3500 V; 0; −1650 V; −3500 V). The left-hand side panels characterize the ion-dominated layers, located at both ends of the sheath, while the right-hand side panels represent the thin electron-dominated layer near $x = 0$. Boundary conditions typical in the Earth's outer magnetosphere and plasma sheet are given in Table 1. It can be seen that the presence of a plasma boundary concentrate the imposed electric potential over a small scale size and gives rise to localized potential differences much larger than that produced by the contact between the two plasmas alone (solid curve ϕ_2 = 0 V).

structures (e.g., illustrated by *Parks et al.* [1992]). On the basis of the results obtained here one would expect that the large-scale potential imposed across the magnetosphere would distribute itself in a higher structured manner with large electric fields and potential differences appearing at multiple plasma boundary locations and small electric fields over intervening regions where the plasma was uniform.

Lyons [1981] has demonstrated that the existence of a large potential difference applied over a small-scale size transverse to the magnetic field in the outer magnetosphere is a sufficient condition for the creation of large magnetic field-aligned potential difference between the outer magnetosphere and the ionosphere in the sense to accelerate electrons downwards. Any magnetospheric electrons scattered into the atmospheric loss cone will be energized and precipitated to produce aurora.

We have shown that the plasma populations within the transition region are likely to produce a wide variety of waves which can scatter the electrons into the atmospheric loss cone. Moreover, the modeled scale sizes of the potential distributions transverse to the magnetic field in the outer magnetosphere are no greater than 500–800 km and exhibit structure on even smaller dimensions. Such scale sizes map from the outer magnetosphere to dimensions of tens of kilometer at ionospheric altitudes, dimensions consistent with those of auroral displays. Because the scale size of the transition regions between plasmas is appropriate to auroral arc dimensions, because the electric potential differences across such boundaries are consistent with those required to account for the energized electrons associated with discrete auroral arcs (much enhanced by the large-scale potentials

applied across the magnetosphere), and because wave particle interactions within the transition regions likely produce pitch angle scattering we conclude that plasma boundaries are the location and source of electromotive force required to produce discrete aurora.

4. Discussion and Summary

This paper has presented the results of a self-consistent calculation of the electric field and plasma structures across the boundary that separates magnetized plasmas of differing temperatures and densities. The plasma parameters were chosen to be typical of the magnetosphere and many features appearing in the results are pertinent to magnetospheric processes, specifically the origin of discrete auroral arcs. These features bear further discussion.

1. The electric potential distribution, $\phi(x)$, across the boundary between the two plasmas is not constant, even when the electric potentials far from the boundary at $x = +\infty$ and $x = -\infty$ are both assumed to be zero. Indeed, the results show that in this case electric potential differences of more than 1000 V arise within the boundary as a consequence of charge separation. This indicates that the solutions obtained by *Harris* [1962], *Alpers* [1969], or *Channell* [1976], for a plasma layer where it was assumed that $\phi(x) = 0$ everywhere, are by no means general solutions. Our model is also more general than that of *Romero et al.* [1990] who have studied a one-dimensional slab Vlasov equilibrium for the plasma sheet boundary layer–lobe interface, by considering the particle guiding center as an approximate constant of motion. Unlike our model, that of Romero et al. is only valid for transitions where the diamagnetic effects can be neglected, i.e., for low plasma β values, and does not permit considering nonzero electric potential differences between $x = +\infty$ and $x = -\infty$. In our model the solution for cases where a non-zero electric potential difference between $x = +\infty$ and $x = -\infty$ is imposed shows that a major portion of the available electric potential appears across the plasma transition region. In such a case the potential difference across the region of the transition can be much larger than that created solely by the plasma discontinuity. Thus these results suggest that whenever the Earth's magnetospheric plasma exhibits internal structure, such as density or temperature variations, the electric potential caused by the solar wind's interaction with the geomagnetic field will not be distributed uniformly across the system but, rather, will distribute with large electric fields, and corresponding large potential differences, at the interface between differing plasmas.

2. The characteristic scale lengths of the plasma and electromagnetic field variables across the transition regions are of the order of the average ion Larmor radius for the larger structures and the average electron Larmor radius for the thinner embedded electron sheaths. The broader scale size is typically 500–800 km near the equatorial plane of the magnetosphere where the local magnetic field strength is 40 nT or less. This scale size, when projected along the magnetic field line to the ionosphere, is reduced by at least 30-fold, i.e., to a dimension of 15–30 km. This dimension agrees quite well with the latitudinal extent of inverted-V regions and discrete auroral arcs. Electric potential variations over much smaller dimensions, of the order of 10 km, are associated with electron-dominated layers. These small dimensions correspond to a fraction of a kilometer when mapped to ionospheric heights and can account for the observed small-scale structure within arcs. The smaller characteristic scale lengths of the electric potential variation correspond to $D_e = \rho_e$ and characterize the electron-dominated layers illustrated in Figures 1–3. Note that the model permits intermediate scale lengths $\rho_e \leq D_e \leq \rho_p$ that correspond, in effect, to a broadening of the central electron layer. Particle gyroradius has also been introduced as a lower characteristic transverse scale length by *Cole* [1991] to determine "upper limit" values for field-aligned current intensity in the polar magnetosphere. Note, however, that this issue is different from that discussed in our quantitative kinetic model.

Lyons [1981] has shown that the existence of large electric potential differences, over small dimensions transverse to the magnetic field in the outer magnetosphere, is a necessary and sufficient condition to account for electric potential differences distributed along the magnetic field lines connecting that region with the ionosphere. Such potential differences along the magnetic field lines are believed to be responsible for accelerating magnetospheric electrons downwards to produce the discrete aurora.

We have shown that magnitudes of the potential differences across the boundaries between plasmas in the magnetosphere are consistent with those potentials required to account for auroral arcs. Moreover, we have shown that the spatial dimensions over which these potentials are distributed transverse to the magnetic field in the outer magnetosphere are similar to those required by Lyons to account for electron acceleration into the atmosphere. For these reasons we conclude that the potential variation across the boundaries between differing plasmas in the magnetosphere should be identified with the source of EMF required to create auroral arcs.

3. We have modeled the plasma and field variations across a magnetospheric plasma boundary for the case where currents in the boundary are perpendicular to the electric fields. In effect, this is an "unloaded" source of EMF and no energy dissipating currents are flowing. The actual acceleration and precipitation of electrons to create an auroral arc requires that a current system be established that threads both the source of EMF and the ionosphere by means of magnetic-field-aligned currents. Figure 4 illustrates the plasma discontinuity generating an EMF at the surface of a plasma sheet density irregularity, and its projection in the terrestrial ionosphere.

In section 3 it was shown that the rapidly convecting plasma populations associated with the electron layer of the boundary were unstable and turbulent wave fields would be produced in this region. It is not unlikely that instabilities would occur over much of the spatially broader ion layer as well. We expect that the presence of turbulent wave fields will scatter electrons into the atmospheric loss cone so that they will be accelerated and precipitated to produce aurora. Moreover, the same wave fields will pitch angle scatter charged particles that originate from the ionosphere out of their source cone so that a current system threading both the EMF and the ionosphere by means of field-aligned currents will be established.

Of course, when a dissipative current system is established, the plasma and field structures across the boundary will be altered from those we calculated. Eventually, the loss

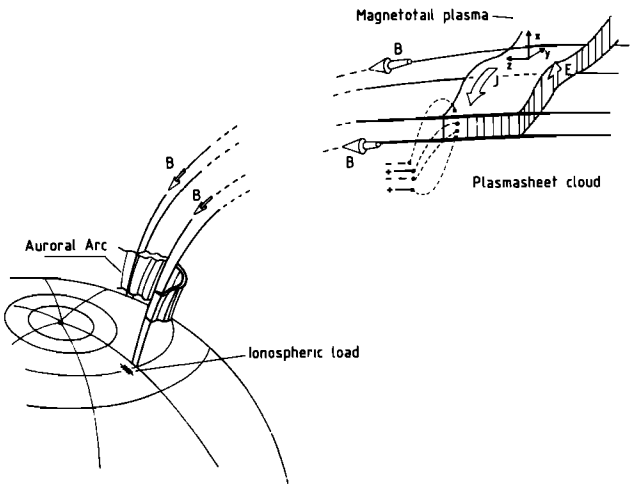

Fig. 4. Illustration of the plasma discontinuity (in this case a tangential discontinuity) generating an EMF at the surface of a plasma sheet density irregularity (cloud or plasma sheet-lobe boundary), and its projection in the terrestrial ionosphere. Electric potential differences are produced by thermoelectric charge separation at the interface between the two plasma regions and are distributed transverse to the magnetic field in the x direction. These potential differences map down into the ionosphere and drive Pedersen currents, provided the local ionospheric conductivity is large enough, i.e., that the system becomes loaded. Because of microinstabilities in the interface region, electrons are scattered in the loss cone; they enhance the ionization at low altitude and increase the Pedersen conductivity. Large Pedersen currents flow in the ionosphere. The diminution of the resistivity reduces electric potential gradients in the ionosphere and leads to the formation of field-aligned double layers such that the circulation of the electric field along the whole circuit is equal to zero (assuming a time-independent magnetic field distribution). The field-aligned potential drop accelerates the scattered and precipitating electrons to several kiloelectron volts. An auroral arc is formed by the bombardment of these electrons in the atmosphere. This produces an additional enhancement of the ionospheric conductivity, smaller ionospheric potential differences but larger field-aligned ones. Provided the plasma cloud in the magnetosphere is a large reservoir of electrons or if the cloud is propagating in the $+x$ direction, the source of precipitated electrons is constantly fed and the auroral arc lasts as long as a large EMF is maintained in the magnetotail.

of energetic charged particles through precipitation, the energy dissipation associated with producing the aurora, and Joule losses from current flowing in the ionosphere will reduce the temperature and density gradients across the magnetospheric plasma boundary we have modeled to the point that the potential distribution is no longer an effective source of EMF.

The time scale required for gradients in the magnetospheric plasma temperatures and densities (and, thus the boundary itself) to dissipate may be estimated from the time required to discharge these particles into the ionosphere. The rate at which electrons are lost from a population with a temperature of 2.5 keV and density of 0.5 cm^{-3} (assuming a full loss cone and no field-aligned electric fields that would enlarge the loss cone) is 4×10^{12} m^{-2} s^{-1} calculated at ionospheric heights. The presence of a large potential difference that widens the loss cone for electrons may increase this loss rate by a factor of 10 [*Lyons*, 1981]. The volume of a $L = 8$ flux tube in a dipolar geomagnetic field with an ionospheric footprint of 1 m^2 is about 10^{12} m^3 and would contain about 5×10^{17} electrons. Even at a loss rate enhanced by significant potential differences along the field line to the ionosphere, it would require >1000 s to reduce the original number density by a factor of 2.

There is also the possibility that a plasma sheet cloud (of finite extent in the y direction) moves transverse to the magnetic field (in the direction of the plasma gradients, i.e. in the x direction), by means of an electric polarization and its associated $\mathbf{E} \wedge \mathbf{B}$ drift. This is for instance the case of a solar wind plasmoid impulsively penetrating into the magnetotail, in the $-x$ direction of the local coordinate system (see Figure 4). Consequently, there is an additional electric field in the y direction, i.e., in the same direction as the current density. Indeed, when the plasma dielectric constant is much greater than unity, collective plasma effects lead to the accumulation of polarization charges along the lateral (x-z) surfaces of the cloud, which generate an internal electric field (in the y direction) inside the moving plasma element (for recent reviews of the theory of impulsive penetration, see *Lemaire and Roth* [1991], and *Roth* [1992]). During the time the plasma cloud is penetrating into the magnetotail, gradients of plasma density, pressure, . . . , are continually re-forming, by means of plasma transport across the x-y surface. The continual re-formation of these gradients maintains the source of EMF. Typical nonadiabatic slowing down times of solar wind plasmoids injected into the magnetosphere have been calculated by *Lemaire* [1977]. These characteristic times depend on the value of Σ_p, the integrated ionospheric Pedersen conductivity. They range from 3 min ($\Sigma_p = 2$ mho) to 30 min ($\Sigma_p = 0.2$ mho), in the case of a solar wind plasmoid with an excess density $\Delta n/n = 5\%$, moving in the solar wind with a velocity of 400 km/s, and having a characteristic scale length (in the y direction) of 10,000 km.

It is also of interest to examine the possibility that electric charge flowing to and from the ionosphere will cancel the unbalanced space charges in the boundary layer and so "short" the large electric fields and potential differences in the boundary region. Panel c_1 in Figure 1 shows that within the broader scale ion layer of the transition region the departure from charge neutrality is of the order of 1–2 $\times$ 10^{-6} or about 1 excess elementary charge m^{-3} (the departure from charge neutrality in the electron region is considerable higher—see panel c_2 of Figure 1). Thus we expect that a 1-m^2 flux tube would depart from charge neutrality by about 10^{12} elementary charges. It would be a mistake, however, to conclude that the excess charge within this entire flux tube would be electrically canceled by a current flow of 1.6×10^{-7} A/m^2 lasting for only 1 s. This would presume that the excess charge were the property of single, identifiable charged particles in the magnetosphere which, if they were removed or electrically canceled, would "short" all charge separation electric fields. In reality, the local charge imbalances within the transition layer between two different magnetospheric plasmas are a property shared among all the charged particles and removing just a single particle will not remove the charge imbalance. The lifetimes of the charge separations and associated electric fields are governed by the time needed to destroy the plasma temperature and density gradients which define the very existence of a boundary. It is this feature of the physical system we have modeled that distinguishes it as being a source of EMF and not simply a charged capacitor.

Our analysis of the electrical structure of magnetospheric plasma boundary layers is summarized as follows:

1. The existence of two plasmas populations that interface with one-another leads directly to the creation of a space-charge separation and electro-static potential difference in a direction normal to **B**. The potential distribution is highly structured with essentially two different scale lengths of variation.
2. The characteristic scale lengths of the plasma and field variables are the average ion Larmor radius (or some multiple of this length) for the broad ion-dominated layers located at the outer edges of the transition and the average electron gyroradius (or some multiple of this length) for the central electron-dominated layer.
3. For plasma parameters pertinent to the Earth's outer magnetosphere and plasma sheet, the largest modeled scale size of the potential distribution transverse to the magnetic field is appropriate to auroral arcs dimensions; while the smallest modeled scale size can account for the observed small scall structure within arcs.
4. When a large-scale potential difference externally imposed across the transition layer is applied, the imposed electric field is concentrated at the interface. This gives rise to localized potential differences much larger than that produced by the contact between the two plasmas alone. Thus the total available solar wind imposed potential difference is reordered by the plasma populations to give rise to large potential differences appearing over small distances perpendicular to **B**—just the situation needed for the creation of an auroral arc.
5. For plasma parameters pertinent to the Earth's outer magnetosphere and plasma sheet, the electric potential differences across the transition layer are consistent with those required to account for the energized electrons associated with discrete aurora—much enhanced by the large-scale potentials applied across the magnetosphere. These electric potential differences can be identified with source of EMF required to create auroral arcs.
6. Waves with spectrum near the lower hybrid frequency are likely to be generated. These waves scatter the pitch angles of electrons into the atmospheric loss cone and establish the current system threading both the EMF and the ionosphere by means of field-aligned currents. Dissipation processes will not change significantly the available potential and electric field intensities of the initially unloaded EMF, as long as the gradients in temperatures and densities are maintained, i.e., during a time interval of at least 1000 s, the estimated half lifetime of the transition.

APPENDIX A

The Vlasov kinetic approach is used to study the transition layer separating a hot plasma sheet cloud from the cooler background. An one-dimensional plane tangential discontinuity (TD) is considered which is parallel to the y-z plane. In this model all plasma and field variables depend only on the x coordinate, normal to the layer. The plasma is assumed to be uniform for large negative and positive values of x, i.e., respectively, deep inside the plasma sheet cloud and far from the cloud in the magnetotail background. Because a TD has no normal component of the magnetic field, the latter lies entirely in the y-z plane, while the electric field **E** is parallel to the x axis. Here we also assume that the magnetic field **B** remains everywhere parallel to the z axis, i.e., $\mathbf{B} = B_z\mathbf{e}_z(B_z > 0)$. Because of the orientation of **B** and **E**, the z velocity component for a charged particle is a constant and we are therefore free to consider the motion of this particle to be in the $(x$-$y)$ plane. In this plane, a single plasma particle is characterized by two constants of motions: the Hamiltonian (H)

$$H = m(v_x^2 + v_y^2)/2 + q\phi \tag{A1}$$

and p_y, the y component of the canonical momentum

$$p_y = mv_y + qa_y \tag{A2}$$

In these equations, q is the charge of the particle of mass m and $\mathbf{v}(v_x, v_y, v_z)$ its velocity vector, while $\phi(x)$ is the electric potential and a_y the y component of the vector potential $[B_z(x) = da_y/dx]$.

Because z is an ignorable coordinate, the velocity distribution function (f) of a given plasma species can be considered only in the $(v_x$-$v_y)$ plane. It is then a function of x, v_x and v_y. On the other hand, any function $f(H, p_y)$ is a solution of the time-independent Vlasov equation. To evaluate moments of f, we have to transform the $(v_x$-$v_y)$ plane to the $(H$-$p_y)$ plane. Each half of the $(v_x$-$v_y)$ plane corresponding to $v_x < 0$ or $v_x > 0$, is mapped into the same domain, given by

$$-\infty < p_y < +\infty,\ H_0 \le H < +\infty \tag{A3}$$

with

$$H_0(p_y, x) = q\phi(x) + \frac{1}{2m}[p_y - qa_y(x)]^2 \tag{A4}$$

Macroscopic plasma parameters like the partial number densities n_i, the $(y$-$)$ components of partial current densities j_i or mean velocities $u_{y,i}$ can then be obtained from f_i as functions of a_y and ϕ (the subscript i characterizes the 2 particle species considered here: $i = e$ for electrons, $i = p$ for protons).

From (A4) the energy equation (A1) can also be written as

$$H = \frac{1}{2}mv_x^2 + \frac{1}{2m}(p_y - qa_y)^2 + q\phi = \frac{1}{2}mv_x^2 + H_0(p_y, x) \tag{A5}$$

From (A3) and (A5) it can be seen that the motion is that of a particle in the potential well H_0. This means that the entire motion of a particle with constants H and p_y lies within the bounded interval on the x axis determined by $H_0(p_y, x) \le H$. There are therefore no particles able to escape at $x = \pm\infty$. As $f(H, p_y)$ can be chosen as an arbitrary function of its arguments it depends no longer explicitly on x. However, the number of trajectories with a given H and p_y determines the number of particles on the x interval determined by $H_0(p_y, x) \le H$.

Let us consider the following velocity distribution functions:

$$f_i = f_{ci} + f_{bi}$$

$$= \frac{m_i\alpha_{ci}}{4\pi kT_{ci}} \exp\left(-\frac{H_i}{kT_{ci}}\right) \operatorname{erfc}(+\delta_{ci}p_{yi})$$

$$+\frac{m_i\alpha_{bi}}{4\pi kT_{bi}}\exp\left(-\frac{H_i}{kT_{bi}}\right)\operatorname{erfc}(-\delta_{bi}p_{yi}) \quad \text{(A6)}$$

where

$$\delta_{ci}=\frac{1}{q_iB_c\sqrt{D_{ci}^2-\rho_{ci}^2}},\quad \delta_{bi}=\frac{1}{q_iB_b\sqrt{D_{bi}^2-\rho_{bi}^2}} \quad \text{(A7)}$$

$$\rho_{ci}=\frac{\sqrt{2m_ikT_{ci}}}{|q_i|B_c},\quad \rho_{bi}=\frac{\sqrt{2m_ikT_{bi}}}{|q_i|B_b} \quad \text{(A8)}$$

and erfc (ζ) is the complementary error function:

$$\operatorname{erfc}(\zeta)=\frac{2}{\sqrt{\pi}}\int_{\zeta}^{+\infty}\exp(-t^2)\,dt$$

It can be seen that protons and electrons from the plasma sheet cloud (subscript c) have velocity distribution functions (f_{ci}) which tend to isotropic Maxwellians at $x=-\infty$ with temperatures T_{ci} (kT being the thermal energies) and densities (see also (1) and (2))

$$n_{ci}(x=-\infty)=\alpha_{ci}\exp\left[-\frac{q_i\phi(x=-\infty)}{kT_{ci}}\right] \quad \text{(A9)}$$

When $x\to+\infty$, the domain of the velocity space where f_{ci} differ from zero become vanishingly small because a smaller and smaller fraction of protons and electrons from the plasma sheet cloud has large enough gyroradius to penetrate deep into the background magnetotail (subscript b) and $n_{ci}(x=+\infty)=0$. The background magnetotail is populated with electrons and protons of a different origin. The velocity distribution functions (f_{bi}) of these particles tend to isotropic Maxwellians at $x=+\infty$ with temperatures T_{bi} and densities (see also (3) and (4))

$$n_{bi}(x=+\infty)=\alpha_{bi}\exp\left[-\frac{q_i\phi(x=+\infty)}{kT_{bi}}\right] \quad \text{(A10)}$$

When $x\to-\infty$, $f_{bi}\to 0$, because as $x\to-\infty$ only a decreasing number of particles from the background with large enough velocities (and gyroradii) are still able to penetrate inside the cloud. Thus $n_{bi}(x=-\infty)=0$.

The parameters D_{ci} and D_{bi} characterize the "thickness" of each of the four transitions that the different particle populations undergo. From (A7) these parameters can not be smaller than the asymptotic Larmor gyroradii in the field B_c and B_b defined in (A8): ρ_{ci} at $x=-\infty$ and ρ_{bi} at $x=+\infty$. When D_{ci} and D_{bi} shrink to ρ_{ci} and ρ_{bi} respectively, the two complementary error functions in (A6) tend to step functions of the variable p_y. In this case the distribution functions are those introduced by *Sestero* [1964], but generalized here to a nonisothermal plasma. Then, as products of a Maxwellian (the exponential in H) by a step function in p_y, they give conceivably the simplest model describing the sharpest transition layer.

Note that the asymptotic behavior of the plasma distributions depends only on the asymptotic form of $f_{b,c}$ when $x\to\pm\infty$. The form of $f_{b,c}$ for any other x in between is responsible for the shape of the transition profile. Thus the state of the plasma at both ends of the transition region does not uniquely determine the plasma and field variation within the transition. This results from the collisionless and adiabatic nature of the interaction between the plasma particles. To remove the nonuniqueness of the velocity distribution functions, consideration of particle accessibility in phase space must be met [*Whipple et al.*, 1984]. This requires the knowledge of the characteristics of the plasma in the boundary source regions together with the transport mechanisms bringing the plasma to the transition itself. Note that only in the case of a collision-dominated plasma when irreversible processes are important is the transition profile uniquely determined by the boundary conditions.

The moments of f_i (f_i given by (A6)) are integrals over the domain of the (H-p_y) plane defined in (A3). The partial densities $n_i=n_{ci}+n_{bi}$ are zero-order moments; the partial current densities $j_i=j_{ci}+j_{bi}$ are first-order moments; temperatures are second-order moments. They are determined in Appendix B.

APPENDIX B

The mean value $\langle W\rangle$ of a particle velocity function $W(v_x, v_y, v_z)$ can be obtained from the corresponding particle velocity distribution function as

$$n\langle W\rangle=\int_{-\infty}^{+\infty}\int_{-\infty}^{+\infty}\int_{-\infty}^{+\infty}W(v_x,v_y,v_z)F(v_x,v_y)\cdot\sqrt{\frac{m}{2\pi kT}}\exp\left(-\frac{mv_z^2}{2kT}\right)dv_z\,dv_x\,dv_y \quad \text{(B1)}$$

where n is the particle number density and F the velocity distribution function in the (v_x-v_y) plane. In the (H-p_y) plane, F transforms into $f(H,p_y)=F[v_x(H,p_y),v_y(p_y)]$. W transforms into $w(H,p_y,p_z)=W[v_x(H,p_y),v_y(p_y),v_z=p_z/m]$. The integral (B1) becomes then

$$\langle w\rangle=0 \quad \text{(B2)}$$

if W is an odd function of v_x or (/and) v_z, and

$$n\langle w\rangle=2^{1/2}m^{-5/2}\int_{-\infty}^{+\infty}\int_{-\infty}^{+\infty}\int_{H_0}^{+\infty}(H-H_0)^{-1/2}\cdot w(H,p_y,p_z)f(H,p_y)\sqrt{\frac{m}{2\pi kT}}\cdot\exp\left(-\frac{p_z^2}{2mkT}\right)dH\,dp_y\,dp_z \quad \text{(B3)}$$

if W is an even function of v_x and v_z.

If $W=v_x^rv_y^sv_z^t$ where r, s, t are nonnegative integers, then the mean values $M(r,s,t)$ of W are moments of the velocity distribution function of order $r+s+t$:

$$M(r,s,t)=n\langle v_x^rv_y^sv_z^t\rangle \quad \text{(B4)}$$

The moments of f_c and f_b, i.e., respectively $M_c(r,s,t)$ and $M_b(r,s,t)$ can be computed from (A6), (B2), and (B3). It is found ($j=c$ or b)

$$M_j(r,s,t)=0 \quad \text{(B5)}$$

if r or (/and) t is odd

$$M_j(r, s, t) = \frac{\alpha}{\sqrt{\pi}} \frac{r!t!}{(r/2)!(t/2)!} 2^{s-1} \left(\frac{kT}{2m}\right)^{\frac{r+s+t}{2}} \cdot \exp\left(-\frac{q\phi}{kT}\right) J_s(h_j\eta, h_j\xi) \quad \text{(B6)}$$

if r and t are even. In (B6),

$$h_c = 1, \; h_b = -1 \quad \text{(B7)}$$

$$\eta = \frac{q}{|q|} \frac{\rho}{\sqrt{D^2 - \rho^2}}, \; \xi = \frac{a_y}{B\sqrt{D^2 - \rho^2}} \quad \text{(B8)}$$

$$J_s(X, Y) = \int_{-\infty}^{+\infty} \exp(-\zeta^2)\zeta^s \operatorname{erfc}(X\zeta + Y)\, d\zeta \quad \text{(B9)}$$

In particular,

$$J_0(X, Y) = \sqrt{\pi} \operatorname{erfc}(W) \quad \text{(B10)}$$

$$J_1(X, Y) = -R \exp(-W^2) \quad \text{(B11)}$$

$$J_2(X, Y) = \frac{\sqrt{\pi}}{2} \operatorname{erfc}(W) + WR^2 \exp(-W^2) \quad \text{(B12)}$$

where

$$W = Y(1 + X^2)^{-1/2}, \; R = X(1 + X^2)^{-1/2} \quad \text{(B13)}$$

From (B8),

$$\xi(1 + \eta^2)^{-1/2} = \frac{a_y}{DB}, \; \eta(1 + \eta^2)^{-1/2} = \frac{q}{|q|}\frac{\rho}{D} \quad \text{(B14)}$$

Therefore

$$J_0(h_i\eta, h_i\xi) = \sqrt{\pi} \operatorname{erfc}\left(h_i \frac{a_y}{DB}\right) \quad \text{(B15)}$$

$$J_1(h_i\eta, h_i\xi) = -h_i \frac{q}{|q|}\frac{\rho}{D} \exp\left(-\frac{a_y^2}{D^2B^2}\right) \quad \text{(B16)}$$

$$J_2(h_i\eta, h_i\xi) = \frac{\sqrt{\pi}}{2} \operatorname{erfc}\left(h_i \frac{a_y}{DB}\right) + h_i \frac{a_y}{DB}\left(\frac{\rho}{D}\right)^2 \exp\left(-\frac{a_y^2}{D^2B^2}\right) \quad \text{(B17)}$$

Moments up to the second order, i.e., the partial number densities n, the partial current densities j (or partial average velocities u_y) and temperatures θ can be deduced easily from (B6), (B7), and (B15) through (B17). These moments are defined as

$$n = M(0, 0, 0) \quad \text{(B18)}$$

$$j = qM(0, 1, 0), \; u_y = M(0, 1, 0)/n \quad \text{(B19)}$$

$$\theta = (\theta_x + \theta_y + \theta_z)/3 \quad \text{(B20)}$$

$$k\theta_x = m\langle v_x^2 \rangle = mM(2, 0, 0)/n \quad \text{(B21)}$$

$$k\theta_y = m\langle (v_y - u_y)^2 \rangle = m(\langle v_y^2 \rangle - u_y^2) = mM(0, 2, 0)/n - mu_y^2 \quad \text{(B22)}$$

$$k\theta_z = m\langle v_z^2 \rangle = mM(0, 0, 2)/n \quad \text{(B23)}$$

Explicit expressions for n and j can be found in section 2 (see (1)–(8)). The temperatures (θ_x, θ_y and θ_z) are given by the following expressions, valid both for particles from the plasma sheet cloud and background magnetotail:

$$\theta_x = \theta_z = T \quad \text{(B24)}$$

$$\theta_y = T\left[1 - \frac{2m}{qD^2B^2} a_y u_y\right] - \frac{m}{k} u_y^2 \quad \text{(B25)}$$

Acknowledgment. The Editor thanks L. R. Lyons and G. R. Wilson for their assistance in evaluating this paper.

REFERENCES

Alpers, W., Steady state charge neutral models of the magnetopause, *Astrophys. Space Sci.*, *5*, 425, 1969.

Channell, P. J., Exact Vlasov-Maxwell equilibria with sheared magnetic field, *Phys. Fluids*, *19*, 1541, 1976.

Cole, K. D., On the limit of field-aligned current intensity in the polar magnetosphere, *J. Geophys. Res.*, *96*, 19,389, 1991.

Davidson, R. C., N. T. Gladd, C. S. Wu, and J. D. Huba, Effects of finite plasma beta on the lower-hybrid-drift instability, *Phys. Fluids*, *20*, 301, 1977.

Eastman, T. E., L. A. Frank, W. K. Peterson, and W. Lennartsson, The plasma sheet boundary layer, *J. Geophys. Res.*, *89*, 1553, 1984.

Elphinstone, R. D., D. Hearn, J. S. Murphree, and L. L. Cogger, Mapping using the Tsyganenko long magnetospheric model and its relationship to Viking auroral images, *J. Geophys. Res.*, *96*, 1467, 1991.

Harris, E. G., On a plasma sheath separating regions of oppositely directed magnetic field, *Nuovo Cimento*, *23*, 115, 1962.

Huba, J. D., N. T. Gladd, and K. Papadopoulos, Lower-hybrid-drift wave turbulence in the distant magnetotail, *J. Geophys. Res.*, *83*, 5217, 1978.

Lee, L. C., and J. R. Kan, A unified kinetic model of the tangential magnetopause structure, *J. Geophys. Res.*, *84*, 6417, 1979.

Lemaire, J., Impulsive penetration of filamentary plasma elements into the magnetospheres of the Earth and Jupiter, *Planet. Space Sci.*, *25*, 887, 1977.

Lemaire, J., and L. F. Burlaga, Diamagnetic boundary layers: A kinetic theory, *Astrophys. Space Sci.*, *45*, 303, 1976.

Lemaire, J., and M. Roth, Non-steady-state solar wind–magnetosphere interaction, *Space Sci. Rev.*, *57*, 59, 1991.

Lyons, L. R., Discrete aurora as the direct result of an inferred, high-altitude generating potential distribution, *J. Geophys. Res.*, *86*, 1, 1981.

Lyons, L. R., Formation of auroral arcs via magnetosphere-ionosphere coupling, *Rev. Geophys.*, *30*, 93, 1992.

Lyons, L. R., and D. S. Evans, An association between discrete aurora and energetic particle boundaries, *J. Geophys. Res.*, *89*, 2395, 1984.

Lyons, L. R., D. S. Evans, and R. Lundin, An observed relation between magnetic field aligned electric fields and downward electron energy fluxes in the vicinity of auroral forms, *J. Geophys. Res.*, *84*, 457, 1979.

McBride, J. B., E. Ott, J. P. Boris, and J. H. Orens, Theory and simulation of turbulent heating by the modified two-stream instability, *Phys. Fluids*, *15*, 2367, 1972.

Parks, G. K., et al., Low-energy particle layer outside of the plasma sheet boundary, *J. Geophys. Res.*, *97*, 2943, 1992.

Romero, H., G. Ganguli, P. Palmadesso, and P. B. Dusenbery, Equilibrium structure of the plasmasheet boundary layer–lobe interface, *Geophys. Res. Lett.*, *17*, 2313, 1990.

Romero, H., G. Ganguli, Y. C. Lee, and P. Palmadesso, Electron-ion hybrid instabilities driven by velocity shear in a magnetized plasma, *Phys. Fluids*, *4*, 1708, 1992.

Roth, M., The plasmapause as a plasmasheath: A minimum thickness, *J. Atmos. Terr. Phys.*, *38*, 1065, 1976.

Roth, M., Structure of tangential discontinuities at the magnetopause: The nose of the magnetopause, *J. Atmos. Terr. Phys.*, *40*, 323, 1978.

Roth, M., A microscopic description of interpenetrated plasma regions, in Magnetospheric Boundary Layers, edited by B. Battrick and J. Mort, *Eur. Space Agency Spec. Publ.*, *ESA SP-148*, 295, 1979.

Roth, M., La structure interne de la magnétopause, *Mem. Cl. Sci. Acad. R. Belg. Collect. 8°*, *44*(7), 222 pp., 1984.

Roth, M., On impulsive penetration of solar wind plasmoids into the geomagnetic field, *Planet. Space Sci.*, *40*, 193, 1992.

Roth, M., J. Lemaire, and A. Misson, An iterative method to solve the nonlinear Poisson's equation in the case of plasma tangential discontinuities, *J. Comput. Phys.*, *86*, 466, 1990.

Sestero, A., Structure of plasma sheaths, *Phys. Fluids*, *7*, 44, 1964.

Sestero, A., Vlasov equation study of plasma motion across magnetic fields, *Phys. Fluids*, *9*, 2006, 1966.

Whipple, E. C., J. R. Hill, and J. D. Nichols, Magnetopause structure and the question of particle accessibility, *J. Geophys. Res.*, *89*, 1508, 1984.

Wu, C. S., Y. M. Zhou, S. T. Tsai, S. C. Guo, D. Winske, and K. Papadopoulos, A kinetic cross-field streaming instability, *Phys. Fluids*, *26*, 1259, 1983.

Zelenyi, L., R. Kovrazkhin, and J. Bosqued, Velocity-dispersed ion beams in the nightside auroral zone: AUREOL 3 observations, *J. Geophys. Res.*, *95*, 12,119, 1990.

D. S. Evans, Space Environmental Laboratory, NOAA, 325 Broadway, Boulder, CO 80303.

J. Lemaire and M. Roth, Institut d'Aéronomie Spatiale de Belgique, Avenue Circulaire 3, B-1180 Brussels, Belgium.

(Received October 30, 1992;
revised January 4, 1993;
accepted December 3, 1992.)